Composites: Part A 181 (2024) 108137

Contents lists available at ScienceDirect

Composites Part A

journal homepage: www.elsevier.com/locate/compositesa

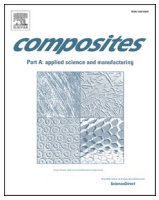

Experimental process characterisation for high-Volume compression moulding of hybrid-architecture composites

Hao Yuan, Muhammad Khan, Ton Peijs, Connie Qian *

WMG, The University of Warwick, Coventry, CV4 7AL, United Kingdom

ARTICLE INFO

Keywords:
Hybrid architecture composites
Compression moulding
High-volume manufacturing
Process characterisation

ABSTRACT

Compression moulding of woven fabric prepreg and sheet moulding compound (SMC) in a single-shot process combines the superior mechanical properties of continuous fibre composites and the high design flexibility of discontinuous fibre composites. This experimental study presents insights into the moulding characteristics of prepreg and SMC and explores the interaction between these two materials during manufacturing of hybrid-architecture composites. All tests were performed under typical compression moulding conditions using a squeeze flow testing rig. The response of each material was interpreted through proposed material models applied to the data acquired from single architecture tests. Critical interaction mechanisms were identified from hybrid architecture tests, alongside some additional deformation mechanisms, such as high level of in-plane fibre tow deformation not observed in single-architecture tests. Novel experimental methods were also introduced to quantify the change in *meso*-scale fibre architecture in the prepreg induced by the flow of SMC. The outcomes of this study not only shed light on the essential interaction mechanisms of hybrid-architecture composites but also provide valuable insights into deformation mechanisms not apparent in isolated material studies. Ultimately, these findings will facilitate the future development of a numerical simulation model for hybrid moulding processes.

1. Introduction

High-volume compression moulding is commonly associated with either continuous fibre based prepreg or discontinuous long fibre based sheet moulding compound (SMC). While continuous fibres as in woven fabrics or unidirectional (UD) tapes can be aligned along the desired loading direction to offer high stiffness and strength, it suffers from poor design flexibility and high material costs, especially for small and complex components. Discontinuous fibre-based SMC offers better design flexibility due to the material's ability to flow, enabling complex geometric features (e.g., ribs and stiffeners) to be manufactured while maintaining low cost and wastage. This enables compensation for the lower mechanical properties resulting from the use of discontinuous fibres through intelligent topology design. Combining these two types of fibre architectures in a single-shot compression co-moulding process can improve the manufacturability of high-performance structural composites by simultaneously offering high structural integrity and design freedom [1–3]. Hybridisation of fibre architectures has been used to combine SMC with dry textile preforms [4] and prepregs [1,2,5], and results showed that tensile properties of these hybrid materials were significantly improved when compared to SMC only counterparts. The increase in stiffness was found to be proportional to the amount of continuous UD prepregs introduced [3,5] while the absorption of impact energy was increased by including discontinuous fibre composites [4].

Understanding the materials' deformation mechanisms in compression moulding of such hybrid-architecture composites is the key for predicting the mould-filling process and the resulting fibre architecture in the manufactured parts. This requires comprehensive studies of the individual material's behaviour, as well as an understanding of the interaction between the materials. Due to the distinctive characteristics in fibre architecture, the compression pressures required for forming and consolidating prepreg (typically < 1 MPa) are usually significantly lower than those for SMC (typically > 20 MPa) [5]. As a result, in-cavity flow of SMC can introduce significant deformation in the continuous fibre preforms, affecting the mechanical performance of the part. In an early study on the influence of SMC flow on the orientation of UD plies during compression moulding, Mallick [6] found that the tensile strength of the hybrid architecture composite in the flow direction

* Corresponding author.
E-mail address: connie.qian@warwick.ac.uk (C. Qian).

https://doi.org/10.1016/j.compositesa.2024.108137
Received 18 October 2023; Received in revised form 6 March 2024; Accepted 9 March 2024
Available online 11 March 2024

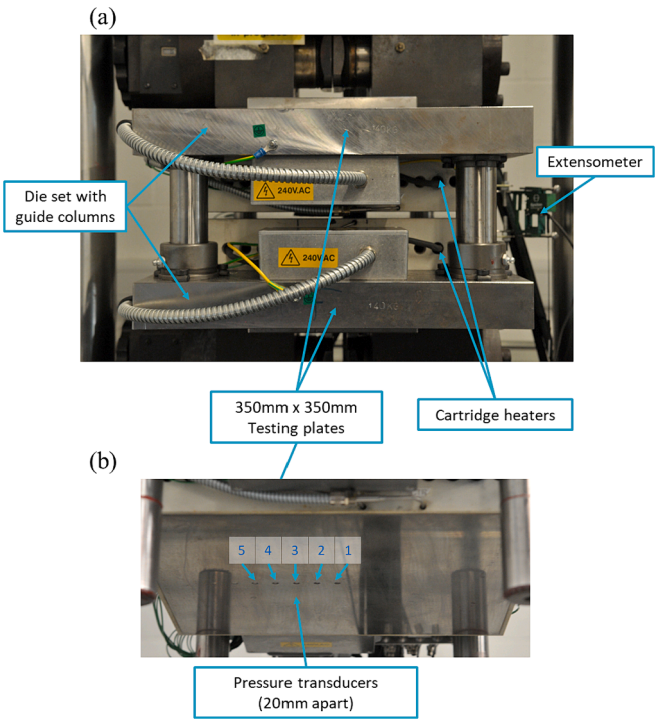

Fig. 1. (a) Squeeze flow rig installed on a servo-hydraulic testing machine and (b) pressure transducers on the upper platens.

decreases with decreased initial coverage of SMC, suggesting that the level of fibre misalignment and distortion is related to the flow length and the location of the charge. Corbridge et al. [5] conducted 1D flow studies on compression moulding of SMC and UD prepreg hybrid architectures with different SMC charge coverage and prepreg ply orientations. By performing grid strain analysis using gridlines that were pre-drawn on the prepreg, it was found that the in-plane fibre waviness in continuous fibres and local fibre volume fraction are affected by the reorientation of the UD fibres to the SMC flow direction, however, B-staging the resin or introducing an inter-ply between the two materials could reduce the distortion of continuous plies. Bücheler [7] proposed using a ferromagnetic filler in the resin to enable magnetic fixation during the compression moulding of hybrid architectures. It was demonstrated that this approach helps to improve the performance and reliability of the components and is a great tool for optimising moulding conditions and the material charge design. All existing studies have focused on different factors that can affect the disturbance to continuous fibres and solutions to minimise these disturbances. However, the fundamental interaction mechanism of how SMC disturbs the continuous fibres is yet to be identified experimentally, although this was claimed to be mainly frictional effects between the different materials [5,7].

Rotational rheometers are widely used in rheological characterisation for polymers due to their high standardisation and low efforts required for data post-processing. Although there was an attempt made to adopt a rotational oscillatory rheometer to characterise SMC [8], this method is generally considered unsuitable for SMCs as the maximum pressure that can be applied with these rheometers (~0.1 MPa) is significantly lower than the pressures required to flow-mould SMC. Other types of commercially available rheometers such as the capillary rheometer or dilatometer were also used for SMC characterisation [9]. However, both types of rheometers can hardly produce representative data due to the limitation of small specimen sizes. The length of fibre bundles in SMC usually ranges from 12.5 to 50 mm [10,11] and it is crucial to have a specimen size greater than the characteristic domain of the SMC. Alternatively, the squeeze flow method can produce a similar flow regime and provide processing conditions that are analogous to an actual compression moulding process, therefore being more suitable for process characterisation of SMCs. The squeeze flow test characterises the SMC flow by compressing the SMC charge between two parallel plates and the strain-rate can be controlled by varying the closing speed of the movable plate. In early 2D squeeze flow tests, cylindrical SMC

Table 1
Specimen configurations and test conditions.

	Configuration 1	Configuration 2	Configuration 3
Layup	1 ply SMC only	1 ply prepreg only	1 ply SMC + 1 ply prepreg
Shape and dimensions	Circular shape with 98 mm diameter	100 mm × 100 mm square	98 mm diameter circular SMC + 200 mm × 200 mm square prepreg
Testing conditions	100 °C 1 mm/s, 3 mm/s, 5 mm/s	100 °C 1 mm/s	100 °C 1 mm/s

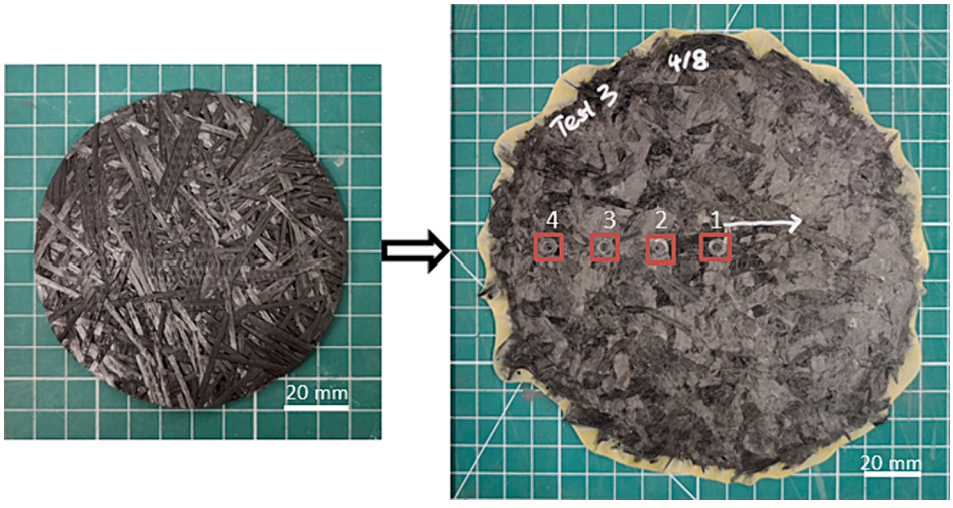

Fig. 2. SMC-only specimen (configuration 1) before (left) and after (right) the squeeze flow test (red boxes indicate the imprints of pressure transducers). (For interpretation of the references to colour in this figure legend, the reader is referred to the web version of this article.)

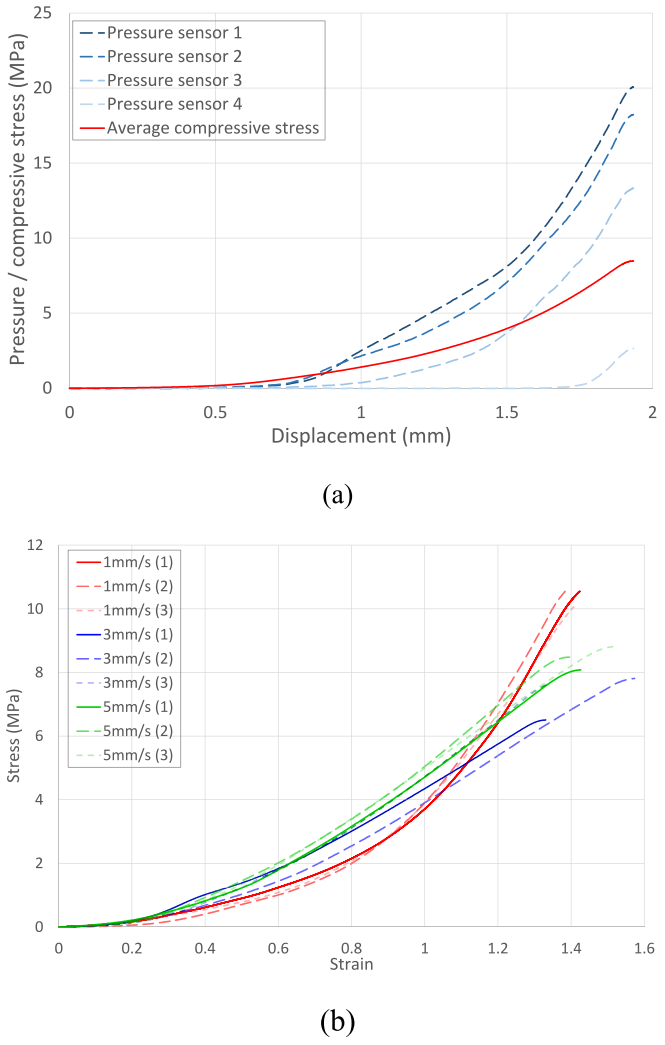

Fig. 3. (a) Average and measured pressure–displacement data for an SMC-only specimen at 100 °C and 5 mm/s, (b) compressive stress–strain curves for all SMC-only tests.

specimens are squeezed between parallel plates and non-lubricated plates [12] or lubricated plates [13] at a range of plate closing speeds and temperatures. These tests were conducted in a constant mass regime (the initial SMC was smaller than the plate size throughout the test) and the applied compressive force and material shear viscosity was found to be strain rate dependent, however, no quantitative data were obtained from these tests and the closing speed was below that of typical compression moulding operations [14]. In a later study [15], the squeeze flow of SMC was investigated at different temperatures and speeds under a constant contact area regime (the initial SMC has the same size as the plates) and material flow was found to be predominantly extensional, based on pressure distribution measurements. However, SMCs have different levels of porosity [16] and under the constant-contact area regime the compressibility of the material during compression or compaction can be hardly investigated. A more recent study using a constant-mass regime [17] demonstrated that the compressibility of the material and the frictional forces between SMC and mould surface can be determined via the in-situ measurement of the normal stress along the radius of the material. To overcome a possible heterogeneous stress state with spatial gradient in a 2D squeeze flow test with cylindrical specimens, the plane strain or 1D squeeze flow test was adopted in some studies to enable a rectilinear and more homogeneous flow [18,19]. The rheological parameters required for the proposed model were determined from the 1D squeeze flow test. Later, Dumont et al. proposed a modified rig that can achieve both 1D and 2D squeeze flow tests [20]. However, latest long fibre SMCs for structural applications have a network of entangled long fibre bundles which complicates their interactions. When subjected to a high compressive force applied over a large surface area during compression moulding, the material deformation is dominated by the compaction of solid-like fibre bundles and the compressive stress [21] rather than shear viscosity in individual fibre suspensions in injection moulding [22].

The characterisation of compaction behaviour for prepreg is usually conducted by compressing the specimen between two parallel heated plates. A review of compaction behaviour for prepregs is presented in [23]. In earlier studies, Chen and Chou investigated the elastic compaction deformation of single-layer [24] and multi-layer [25] woven prepreg in liquid composite moulding processes. The authors proposed an analytical 3D compaction model for predicting the deformation of the specimen and the packing of fibre tows. Later, Comas-Cardona et al. studied the non-linear elastic–plastic compaction behaviour for woven prepreg through loading and unloading the material during the test and proposed a 1D constitutive law with large deformation formulation and measurable parameters to model the through-thickness deformation of the fibre reinforcement during compression [26]. The displacement field within the thickness was considered homogeneous for thick specimens. More recently, a ramp-dwell testing regime with cruciform cross-plied specimens was used to characterise advanced thermoset prepreg in aerospace-related processes, in which the contributions to the compressive stress were separated for fibre bed and resin [27]. This study identified the existence of a transition from percolation flow to squeeze flow and the coupling between two flow regimes during the compaction of prepreg. The characterisation approach was later used to produce the parameters for a phenomenological model predicting the squeezing and percolation flow behaviour of UD [28] and woven prepreg [29]. In more recent studies, the in-plane displacement of fibres in UD prepreg laminates induced by squeeze flow was traced by placing copper wires between plies [30] or using a semi-transparent test rig for real-time full-field measurements [31]. The driving force for in-plane fibre tow washout was identified and localised and the consolidation of the prepreg was modelled via the local modification of material properties [32]. A recent benchmark study [33] investigated the compressibility of woven and non-crimp fabric (NCF) in both dry and wet forms through compaction tests in 26 participating labs. A large scatter in results was found between participants and the major variables in the test and analysis were identified as the thickness measurement approach, the method for machine compliance correction and parallelism, and the level of specimen saturation in the resin. However, these existing characterisation programmes are limited to either low-rate or low-pressure conditions and the compaction behaviour of prepreg in a high-volume compression moulding setting is yet to be investigated in detail.

This study aims to identify critical deformation mechanisms for continuous fibre-based woven prepreg, discontinuous fibre-based SMC and the interaction properties between the two materials in a high-volume hybrid architecture compression moulding process. Experimental material characterisation was performed under typical compression moulding conditions using a squeeze flow testing rig. Compressive stress–strain curves were derived for prepreg and SMC through the single architecture tests, to interpret the constitutive behaviour of each individual material. Critical interaction properties between the two materials were identified in the hybrid-architecture tests, along with additional deformation mechanisms in each of the individual materials that could not be captured in the single architecture tests. Meso-scale fibre architecture in the prepreg was studied before and after each test through micrographs and the grid strain analysis (GSA) method to understand the influence of compaction and the flow of SMC. The findings from this work can facilitate the future development of a numerical simulation model for compression moulding of hybrid architecture composites.

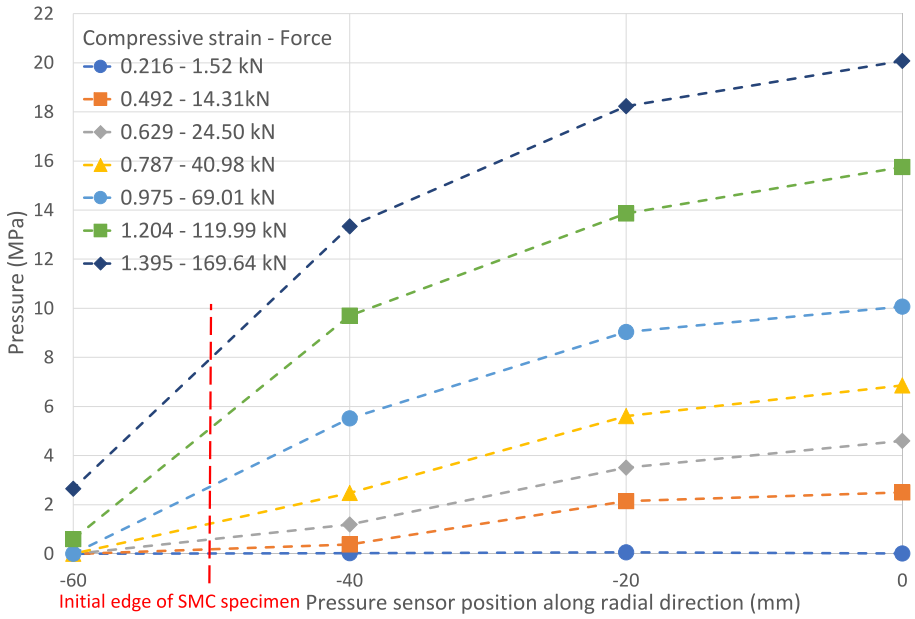

Fig. 4. Pressure measurements along the radius during the squeeze flow test for an SMC-only specimen at 100 °C and 5 mm/s.

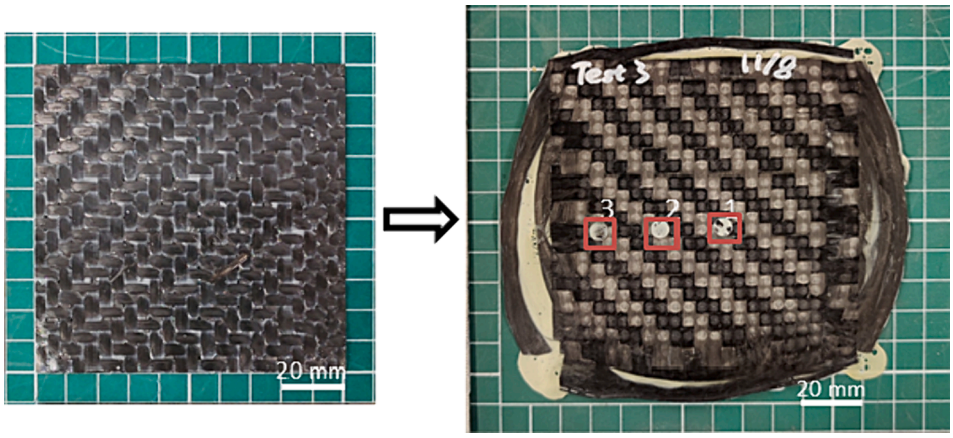

Fig. 5. Prepreg-only specimen (configuration 2) before (left) and after (right) the squeeze flow test (red boxes indicate the imprints of pressure transducers). (For interpretation of the references to colour in this figure legend, the reader is referred to the web version of this article.)

2. Experimental methodology

2.1. Materials

Both prepreg and SMC materials used in this study were supplied by DowAksa (Turkey) and consisted of high-strength carbon fibre and compatible epoxy resin systems. Both resin systems were specially developed for high-volume processing with a cure time of 2 min at 150 °C. The prepreg had VORAFUSE^{TM} P6300 resin, a twill weave with 12 K tows (AKSACA^{TM} A49-D012), 603 gsm areal weight, and 55 % fibre content by weight. The prepreg was not commercially available, therefore further details about the prepreg material cannot be disclosed for reasons of confidentiality.

The SMC was the EMC commercially available through DowAksa, which is a tack-free chopped UD prepreg (AKSACA^{TM} A42-D051 24 K tows) based material consisting of a nominal fibre length of 27 mm (a small amount of tows are above 27 mm long due to missing cuts) and VORAFUSE^{TM} M6400 resin, with 1048 gsm areal weight and 53 % fibre content by weight. In hybrid moulding or SMC compression moulding, the flow distance or the initial coverage of the SMC can range from 20 to 100 % of the final part area depending on the part geometry and material supplier's recommendation [5,34,35]. Meanwhile, the ratio between specimen dimensions and fibre length can play a role in the material response [20]. If the SMC specimen is too small (close or less than the fibre length) the material response during the test will not be representative. Additionally, some of initial trial tests shows that if the SMC specimen is too large and flows beyond edges of the prepreg, the deformation mechanisms of prepreg cannot be fully captured. The combination of specimen dimensions chosen in current study allows an approximately 40 % initial coverage which provides a representative material behaviour while allowing to capture the deformations of the prepreg beyond the SMC flow front.

2.2. Material characterisation

An in-house build squeeze flow rig (Fig. 1 (a)) was used to perform the experimental process characterisation studies to understand the materials' behaviour in a compression moulding process. The rig consisted of two electrically heated parallel platens with 350 mm × 350 mm testing surface area, attached to a die set with four guide columns to ensure parallelism during the test. All tests were performed on a 250 kN servo-hydraulic testing machine. An extensometer of 100 mm gauge

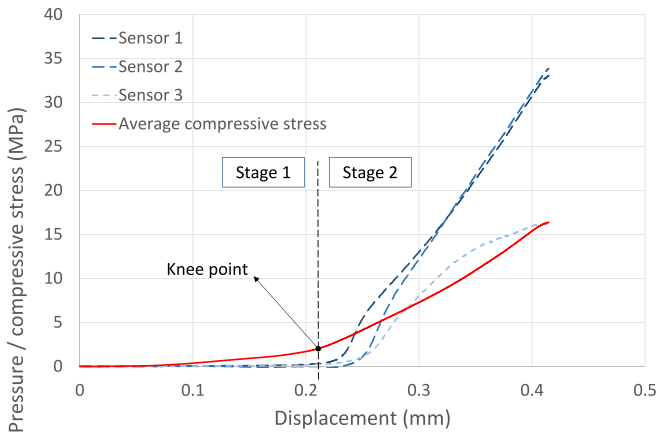

(a)

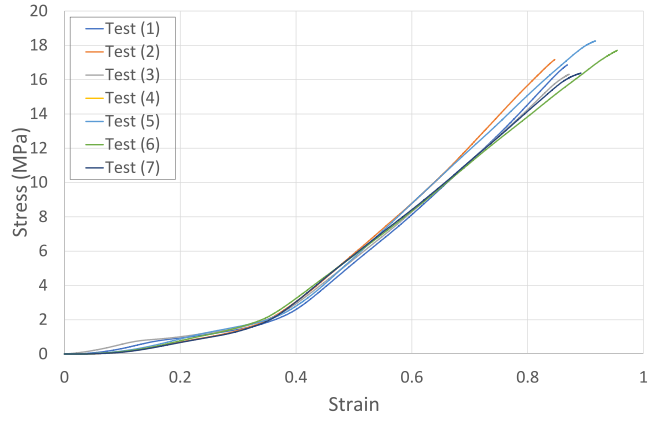

(b)

Fig. 6. (a) Average and measured pressure–displacement data for a prepreg-only specimen at 100 °C and 1 mm/s, (b) compressive stress–strain curves for all prepreg-only test repeats.

length and ± 6 mm range was attached to the parallel platens for directly measuring the displacement of the moving platen. As shown in Fig. 1 (b), there are five pressure transducers with 100 MPa measuring range flush mounted on the top platen from the centre to the edge at an equal interval of 20 mm.

Experimental material characterisation was conducted for single architecture specimens as well as hybrid architecture specimens. Table 1 shows a summary of all types of specimens tested and the relevant test conditions. Five repeats were performed for each specimen type at each test condition. The single architecture specimens (configuration 1 & 2) consisted of a single ply of SMC or prepreg, whereas the hybrid architecture specimens (configuration 3) consisted of a single ply of SMC centrally located at the top of a single ply of prepreg. A testing temperature of 100 °C was adopted for all the specimens because the viscosity of the resin at 100 °C was close to the normal processing temperature (150 °C), but the reaction rate was significantly lower [36], allowing sufficient time for loading the specimen and setting up the test programme. A constant speed profile was applied to all the tests with a 200 kN force limit and 0.1 mm position limit. The moving platen is kept at a gap above the specimen so that the platen can reach the set speed before it starts compressing the material. It is worth noting that the actual cavity height is greater than the crosshead position reading due to the compliance of the testing machine, therefore the readings for the change in cavity height were taken from the extensometer. Once the test was stopped, the specimen would be held in the testing rig at a constant cavity height for 20 min, after which the specimen would reach a sufficient degree of cure to be removed with ease. Partial closure tests, in which the test was stopped at different force levels before the force and position limit, were also performed for prepreg only and hybrid architecture specimens to further examine the material deformation mechanisms at different stages of the test.

Understanding individual constitutive relationships for SMC and prepreg is one of the main objectives of the single architecture tests (configuration 1 and 2). The following assumptions were made for the calculation of through-thickness stress and strain:

1. The material flow is fully homogeneous.
2. At macro-scale of a specimen, the material is compressible and the specimen volume decreases linearly during the test due to the change of packing arrangement of fibre tows and fibre filaments as a result of resin bleeding.

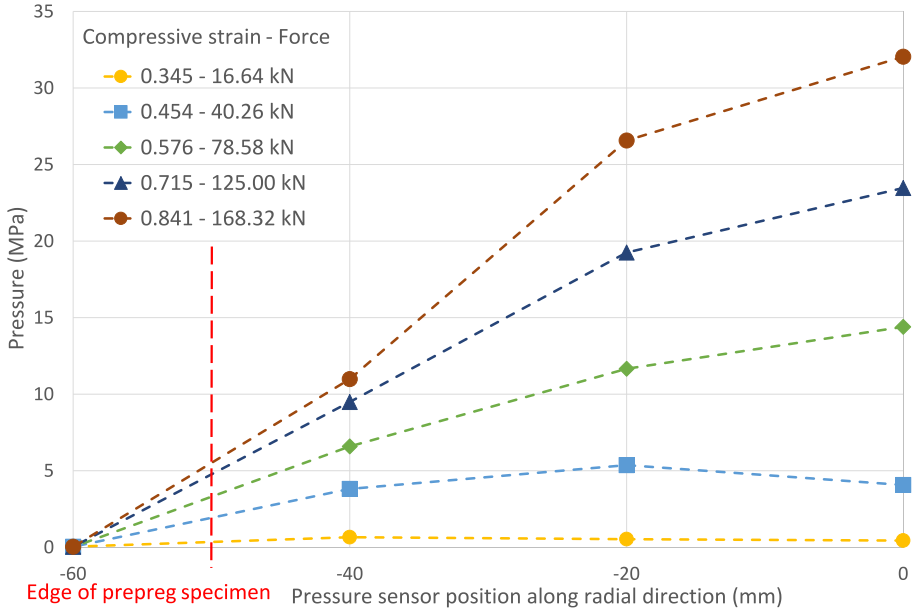

Fig. 7. Pressure distribution from the centre to the edge of the specimen for a prepreg-only specimen at 100 °C and 1 mm/s.

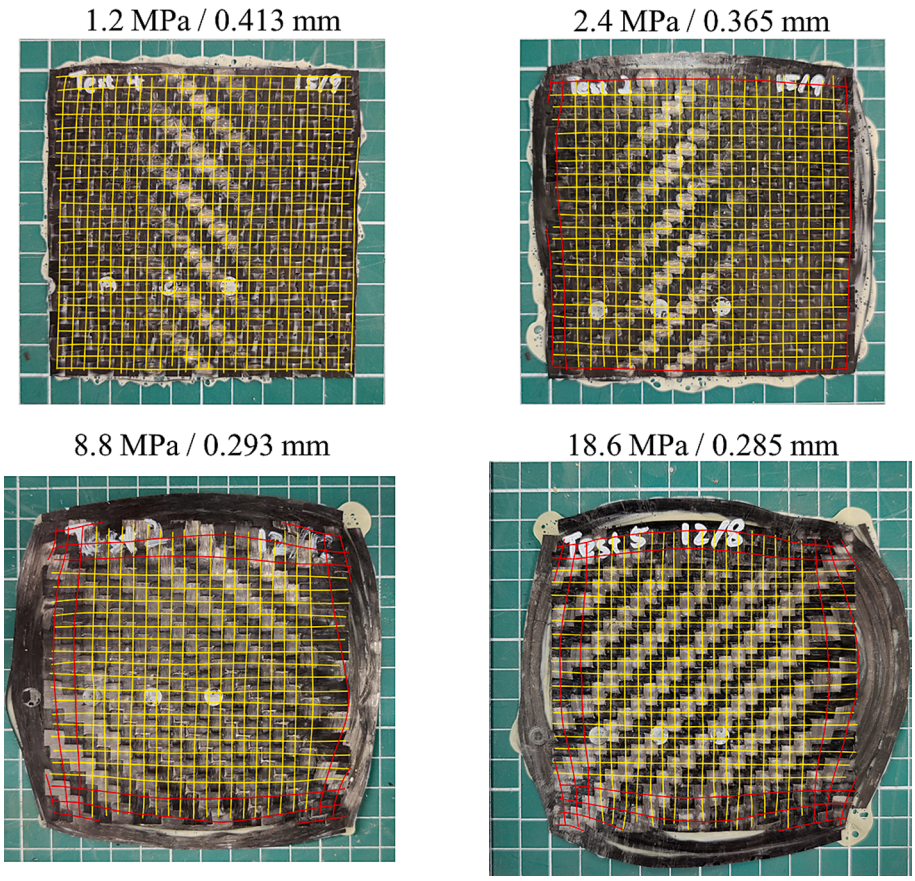

Fig. 8. Centrelines (in yellow and red) of fibre tows in prepreg specimens tested at different compressive stresses with different final thicknesses (partial closure tests). (For interpretation of the references to colour in this figure legend, the reader is referred to the web version of this article.)

3. There is no friction between the specimen and tool surface (perfect slip).

Based on assumption 2 above, the decrease in volume per through-thickness displacement k can be expressed as:

$$k = \frac{V_0 - V'}{h_0 - h'} \tag{1}$$

where V_0 and V' are initial and final volume of the specimen and h_0 and h' are initial and final thickness of the specimen. The thickness of each specimen after the test h' was measured under a Zeiss Axio optical microscope. Due to surface undulation and inhomogeneity of uncured SMC and prepreg, the deviation in initial thickness was very high (2.27 - 3.49 mm for SMC and 0.66 - 0.81 mm for prepreg). Therefore, the initial thickness h_0 and momentary thickness of the specimen during the test h were determined from the change in cavity height measured via an extensometer. While the pressure transducer can detect the flow front at discrete points, the flow front of SMC is not perfectly circular and symmetrical due to the randomness of the fibre architecture. Therefore a field measurement method for the area is considered more accurate. The final coverage area of SMC specimen A' was measured from photographs taken after the test using ImageJ processing software whereas the contact area of prepreg specimen during the test was considered to be constant during the test. Previous studies on the rheology of SMC suggested that the flow behaviour was predominantly plug-flow with a very thin layer of wall-sliding [37,38], and recent models based on these characteristics produced good agreement with experimental data regarding the relative change in volume [39,40]. For the relatively thin specimens tested in current study, the different in calculated volume would have less than 5 % error if the material followed a pure shear flow. Hence, the momentary volume V and momentary contact area A between the specimen and mould surfaces during the test can be calculated as:

$$V = V_0 - k \bullet (h_0 - h) \tag{2}$$

$$A = V/h \tag{3}$$

The through-thickness compressive stress σ_c can then be simply calculated as:

$$\sigma_c = F_c/A \tag{4}$$

where F_c is the compression force obtained from testing machine. The through-thickness compressive strain of the specimen ε_c can be determined:

$$\varepsilon_c = \ln(h/h_0) \tag{5}$$

3. Results and discussions

3.1. SMC-only specimens (configuration 1)

Fig. 2 shows a typical SMC specimen before and after the test. The flow can be considered transversely-isotropic such that the shape of the specimen remained virtually circular after the test. The diameter of the SMC-only specimens with an initial coverage of 35 % increased by an average of 69 % under 200 kN maximum compression force. Resin bleeding was observed around the edge of each specimen at this temperature, although it was assumed that this occurred after the test had stopped, while the specimen was held at a constant cavity height to be cured. To prove this assumption, trial tests were performed at 140 °C

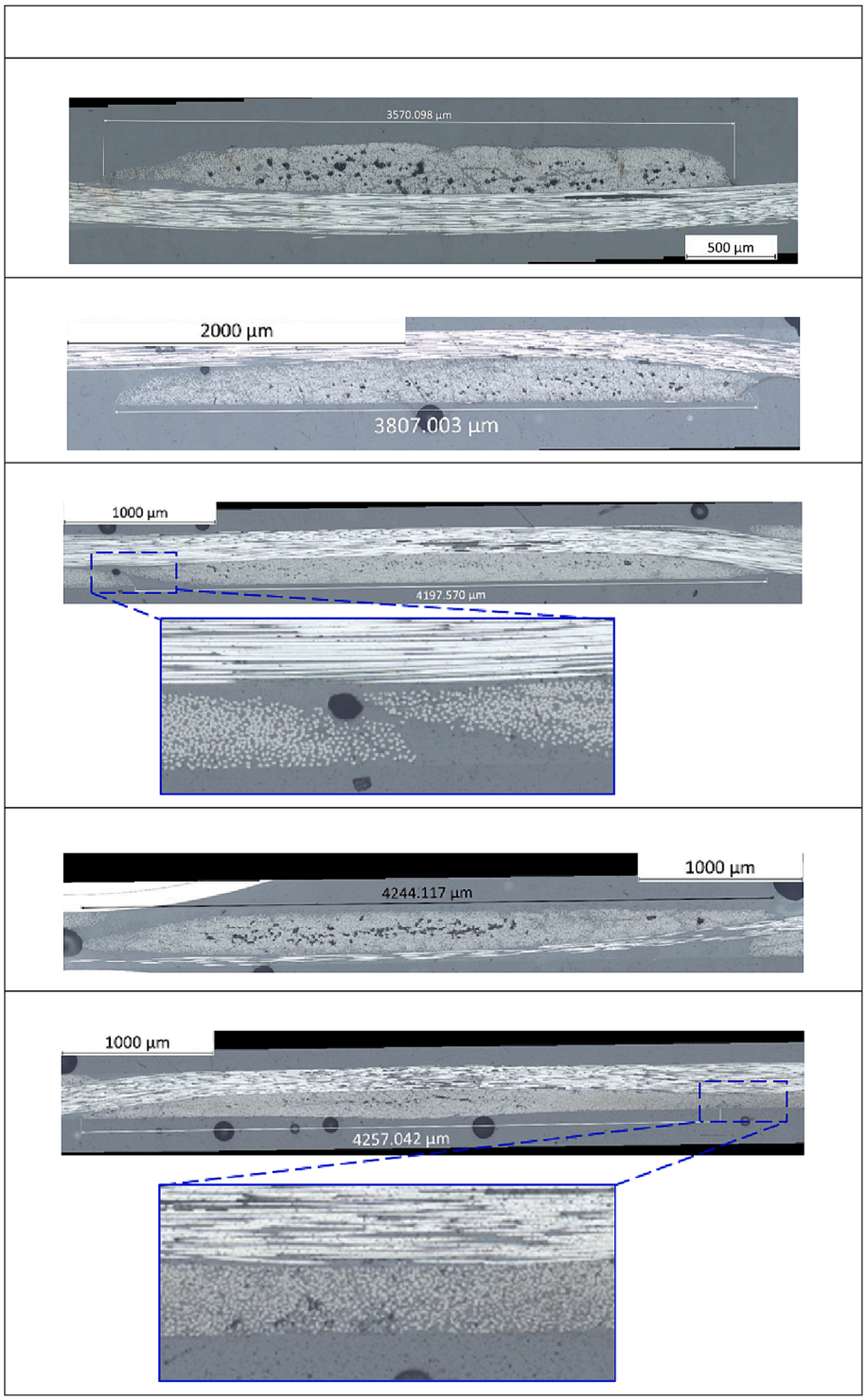

Fig. 9. Micrographs of cross-sections of prepreg-only specimens at different compressive strain/pressure levels.

where the material experienced a much higher curing rate, and no resin bleeding was observed.

Fig. 3 (a) shows average compressive stress (calculated from Eq. (1) - (4)) and the measured pressures at each location against the plate displacements, where the locations of the pressure transducers can be seen from the imprints on the specimen highlighted in Fig. 2. The material exhibited a gradually stiffened response with increasing crosshead displacement. As the pressure transducers are slightly sunken into the mould surface, the pressure readings were only picked up in a later stage of the test when fibre tows in the specimen are closely packed and the small recession above the pressure transducers was filled. Therefore, the increase of pressure readings at the beginning of the test lagged slightly behind the calculated average stress. Fig. 3 (b) presents the compressive stress–strain curves for SMC at different test conditions calculated using Eq. (4) and Eq. (5). SMC shows an overall rate-dependent compressive stress–strain relationship as the compressive stresses increase with test speed. However, the compressive stress for 1 mm/s test was higher at a strain greater than 1.2. Under slower closing speeds, the voids and air between fibres and fibre tows were forced out during the initial stage where the compaction of the material dominates and the material shows

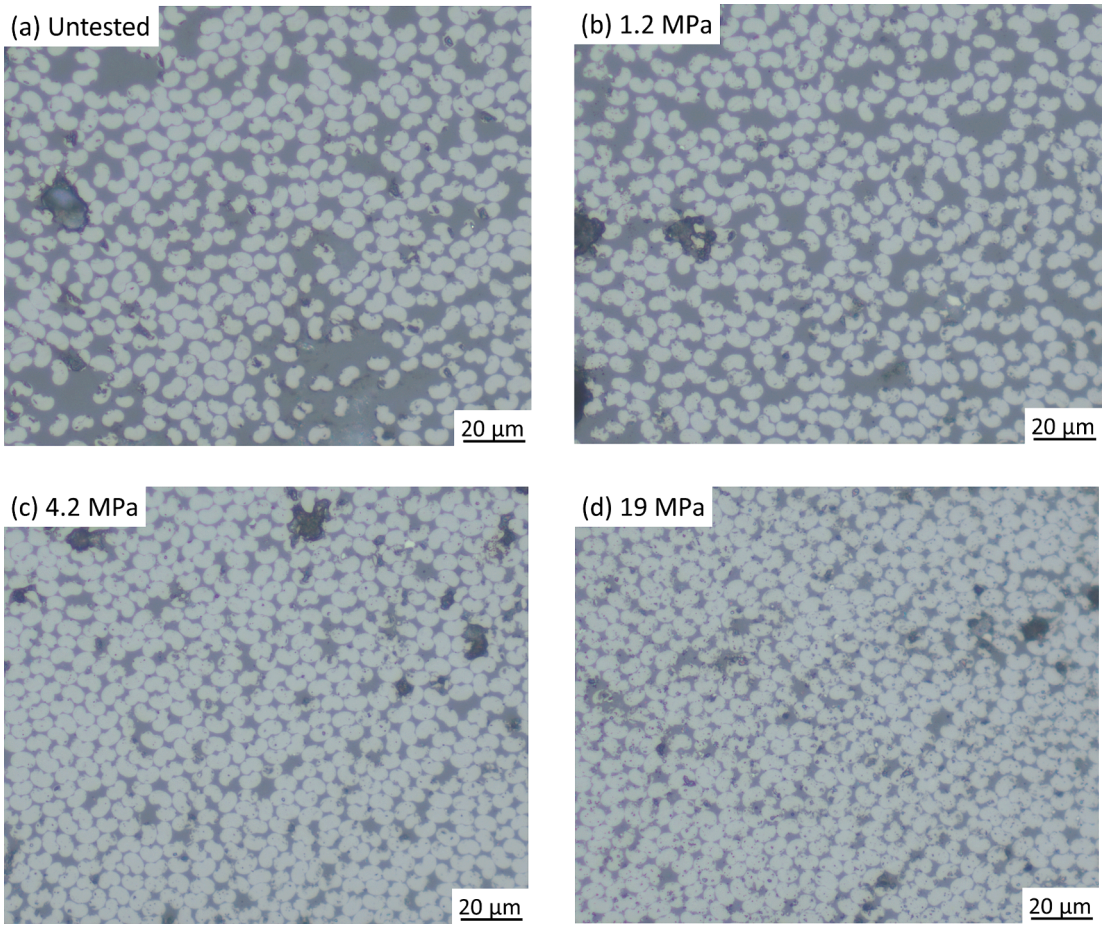

Fig. 10. Examples of higher magnification micrographs of the cross-section of prepreg fibre tows at different levels of nominal pressure.

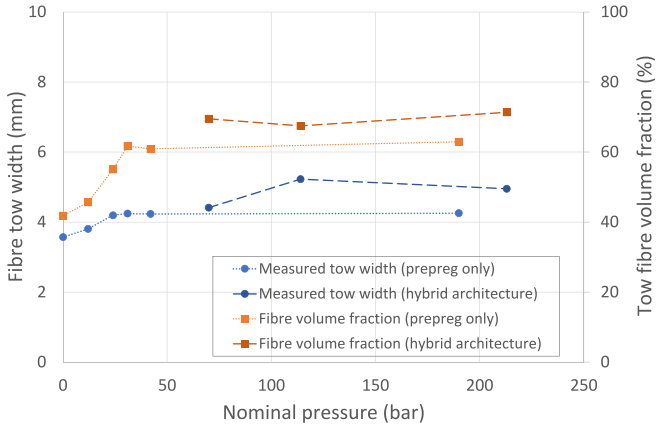

Fig. 11. Average fibre tow width and fibre volume fraction for specimens tested to different levels of nominal pressure.

a foam-like behaviour. At a later stage, the material shows an increasingly stiff response as the SMC starts to flow. However, both compaction and flow took place simultaneously for tests under higher closing speed, therefore, the material shows a more linear response. A similar 'hardening' effect may still be present at higher strains for tests under higher closing speeds as voids and air are escaping from the material, however, tests were stopped before this 'hardening' stage was due to take place as we reached the load limit of the test rig. Fig. 4 compares the pressure distribution along the radius direction from the centre (pressure sensor 1 at 0 mm) recorded at different displacements (forces), where all curves indicate that the pressure decreases from the centre to the edge of the specimen. The pressure gradients between sensor 1 to 3 (0 mm to -40 mm), which were covered by the SMC from the beginning of the test, remained approximately constant during the test (the reading at -40 mm was 56 - 66 % of that at centre of the specimen). It should be noted that sensor 4 at 60 mm had zero reading at small displacements as it was not covered by the material from the beginning of the test.

3.2. *Prepreg-only specimens (configuration 2)*

Fig. 5 shows a typical prepreg specimen before and after the test. Although resin bleeding and fibre wash-out were observed along the specimen edges, no noticeable in-plane displacements were observed for the majority of the fibre tows, therefore no noticeable change was observed in the overall in-plane dimensions of the fibre preform. In Fig. 6 (a), the prepreg shows a bi-linear response as the average stress increases at a higher gradient after the knee point at around 0.2 mm displacement, which correlates to two stages of the specimen deformations discussed later in this sub-section. As the pressure transducers are slightly sunken into the surface of the mould and the thickness of a single-ply prepreg is small, the pressure readings were likely to be inaccurate. This also explains the reason that the pressure readings only started to increase in the second stage of compaction where fibre tows in the prepreg are closely packed. The compressive stress–strain curves for prepreg specimens calculated using Eq. (4) and Eq. (5) are presented in Fig. 6 (b). The woven prepreg again shows a bi-linear stress–strain response with a transition point at around 2 MPa compressive stress (0.35 compressive strain) and a significantly higher gradient at higher stress levels, caused by the transition from bleeding flow to squeeze flow.

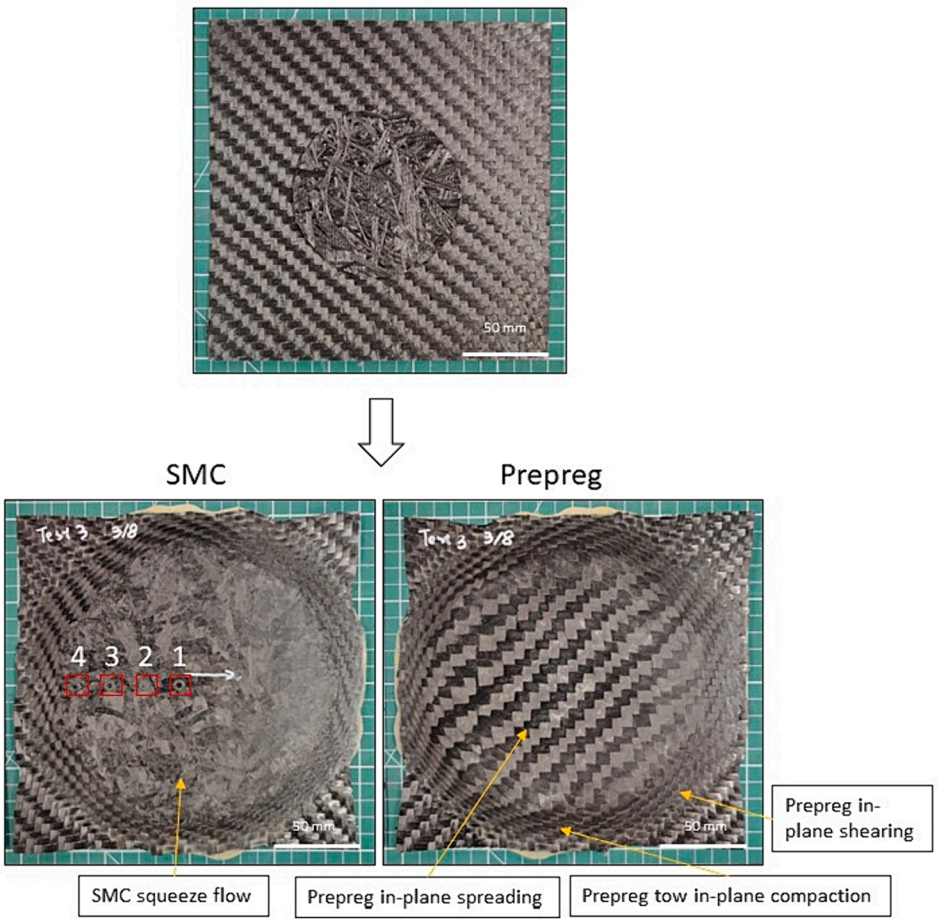

Fig. 12. Hybrid-architecture specimen (configuration 3) before and after the squeeze flow test (red boxes indicate the imprints of pressure transducers). (For interpretation of the references to colour in this figure legend, the reader is referred to the web version of this article.)

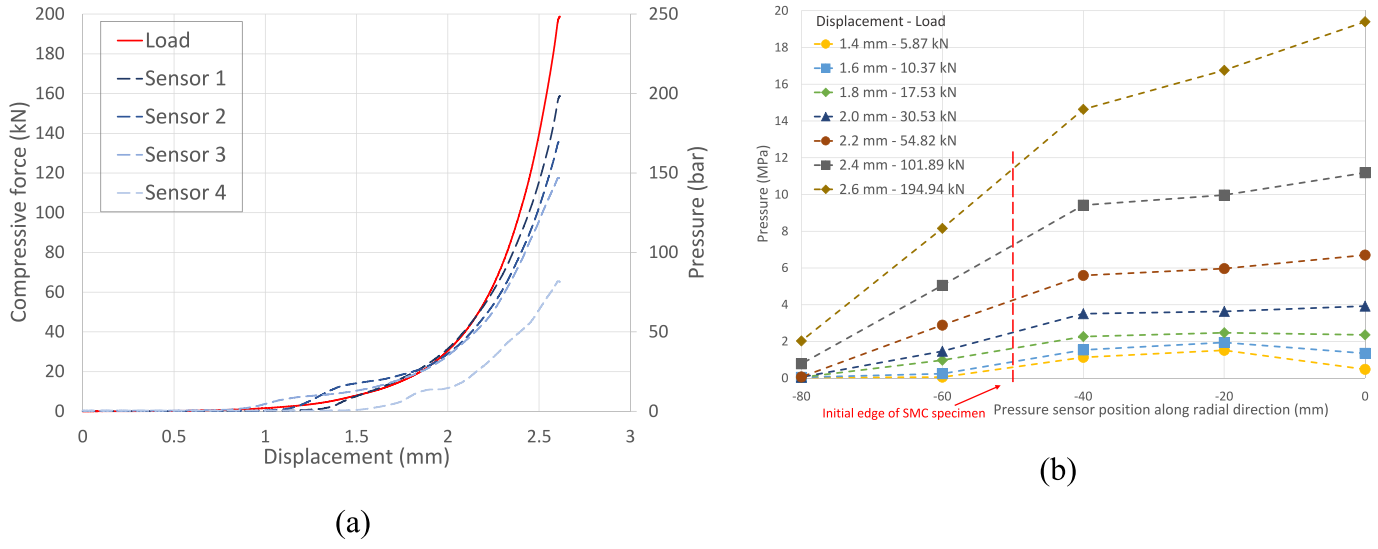

Fig. 13. (a) Compressive force- and pressure–displacement data and (b) pressure distribution along the radius for a hybrid architecture specimen at 100 °C and 1 mm/s.

The pressure distributions from the centre to the edge of the prepreg specimen at different levels of compression are plotted in Fig. 7. Near the knee point (0.345 compressive strain), the pressure remained relatively consistent at around 5 MPa across the three pressure readings. As the specimen was further compressed, a variation in pressure distribution from the centre to the edge started to occur, where the pressure gradient between sensor 2 (-20 mm) and sensor 3 (-40 mm) was noticeably higher than that between 0 mm and -20 mm. Furthermore, the pressure gradient between -20 mm to -40 mm continued to increase with displacement, where there was no noticeable change in the pressure

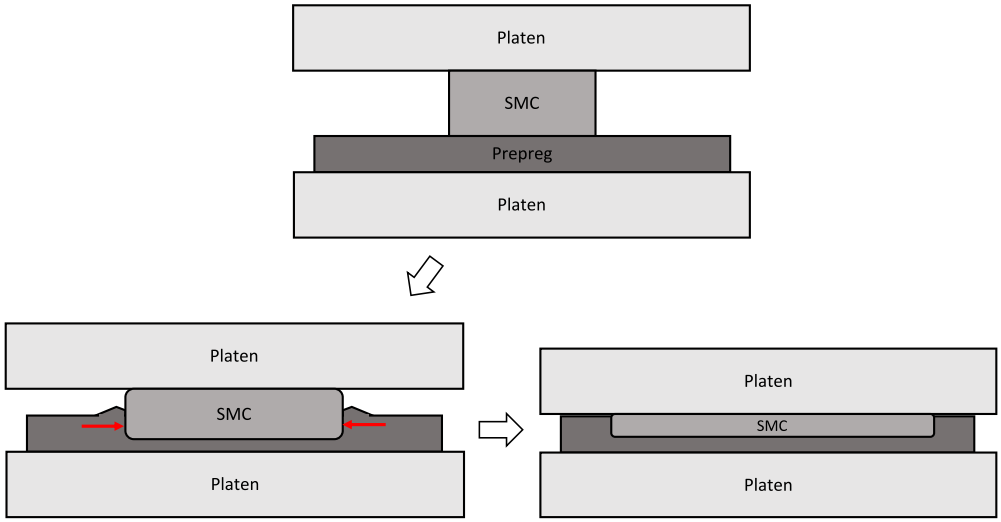

Fig. 14. Schematic illustration of the interaction between SMC and prepreg in the hybrid architecture test.

gradient between 0 mm and -20 mm as a result of the squeeze flow mechanisms in the second stage of compaction. To further investigate the relationship between the pressure distribution and the *meso*-scale deformation of the fibres, Fig. 8 presents a series of specimens which have been tested under different maximum stresses (i.e. partial closure tests), where the centrelines of fibre tows are indicated to help visualise the deformation and displacement of the tows. It can be observed that the fibre tows remained straight without any in-plane displacement with the centreline of each tow remaining in place for specimens tested to the compressive stresses of 1.2 MPa and 2.4 MPa. This suggests that the specimen was experiencing hydrostatic pressure across most surface areas during the first stage where gaps between individual fibres were reduced. For specimens tested at 8.8 MPa and 18.6 MPa maximum stresses, the tows near the specimen edges became curved and diverted away from their original location. This is in line with the hydrodynamic pressure observed between sensors 2 and 3 (-20 mm and -40 mm) caused by the squeeze flow effect [27,31].

The deformation mechanisms for prepreg-only specimen were investigated through microscopic observations, as shown in the cross-section of the specimen tested to different pressure levels (Fig. 9): during the initial compaction up to 0.413 strain, the nominal width of the fibre tows increased from 3.5 mm to 4.2 mm and the edges of adjacent fibre tows remain untouched; after further compaction in the next stage, although there was no further increase in fibre tow width, the profile of the tow flattened and gaps between adjacent fibre tows almost disappeared into very small resin-rich regions.

Micrographs of the cross-section of prepreg fibre tows were taken at a higher magnification with examples shown in Fig. 10. Fibres in the tow become more closely packed as pressure increases, leaving less resin-rich regions towards the end of the test. However, the change in the packing density of fibres was more significant from 0 to 4.2 MPa than from 4.2 to 19 MPa. High magnification micrographs were taken for at least three fibre tows for each partial closure test specimen and the fibre volume fraction in the tow was determined from micrographs using the technique described in [41] with the assistance of ImageJ. The average tow fibre volume fraction of these specimens was plotted in Fig. 11 along with the average tow width. For prepreg-only specimens, the fibre volume fraction in the tows increased significantly from an initial 42 % to 62 % at 3 MPa pressure and showed very little increase during the remaining of the test to a final value of 63 %, as a result of the combined effect of resin bleeding from the specimen [27,28] and the non-linearity of the fibre and tow packing [42]. This is in line with the change of tow width, which increased from an initial 3.6 mm to 4.2 mm at 3.1 MPa and plateaued during the rest of the test with a final width of 4.3 mm. Therefore, the two-stage compaction response of the prepreg-only specimen can be summarised as: in the first stage, gaps between individual fibres are reduced and fibres from the same tows become closely packed at the knee point (change of fibre packing); further compression in the second stage resulted in a change of the fibre tows' profile and movement of tows at the edges of the specimen (change of tow packing).

3.3. *Hybrid-architecture specimens (configuration 3)*

Squeeze flow tests on hybrid specimens involved the moulding of a centrally located single ply of SMC prepreg (~40 % initial coverage) on top of a net-shaped single ply of woven fabric prepreg. Fig. 12 (a) shows a typical hybrid architecture specimen where both sides of the specimen after the test are presented. In this hybrid architecture specimen, the SMC deformed similarly as in an SMC-only specimen and the diameter increased by 61 % after compaction, slightly less than the level of increase for the SMC-only configuration (69 %) (Fig. 2). The overall in-plane dimensions of the woven prepreg in the hybrid architecture specimen remained at 200 mm × 200 mm square whereas *meso*-scale deformation was observed in the prepreg such that the dimensions and the orientation of fibre tows were affected by the SMC flow. Major deformation mechanisms observed in the prepreg include (i) tow spreading (increase in tow width) in the region directly underneath the SMC, and (ii) tow compaction (decrease in tow width) and (iii) in-plane shearing (change in tow orientation) in the region ahead of the flow front of the SMC (see Fig. 12).

Fig. 13 (a) shows the compressive force–displacement curve and pressure history during the test for a hybrid architecture test. Both the force and the pressure curves in Fig. 13 (a) have similar characteristic shapes to those from the SMC-only tests (see Fig. 3 (a)). As shown in Fig. 13 (b), the pressure distributions in the hybrid architecture specimen have a 'bi-linear' shape (a combination of SMC and prepreg effects) compared to the more gradually changed pressure distributions in the SMC-only specimen (Fig. 3 (b)). Compared to the SMC-only test, the pressure was relatively evenly distributed across the central region of the specimen during the hybrid architecture test with a very small pressure gradient from 0 mm to -40 mm up to a displacement of 2.4 mm. This hydrostatic-like pressure in the central region can be attributed to the hybrid moulding effect of SMC and prepreg: the interaction of two deformable fibre architectures imposes greater resistance to the flow compared to a flat and rigid mould tool surface in the SMC-only test, especially the in-plane tow compaction of prepreg near the flow front of SMC. SMC and prepreg directly under the SMC are compacted in the through-thickness direction simultaneously while the rest of the prepreg

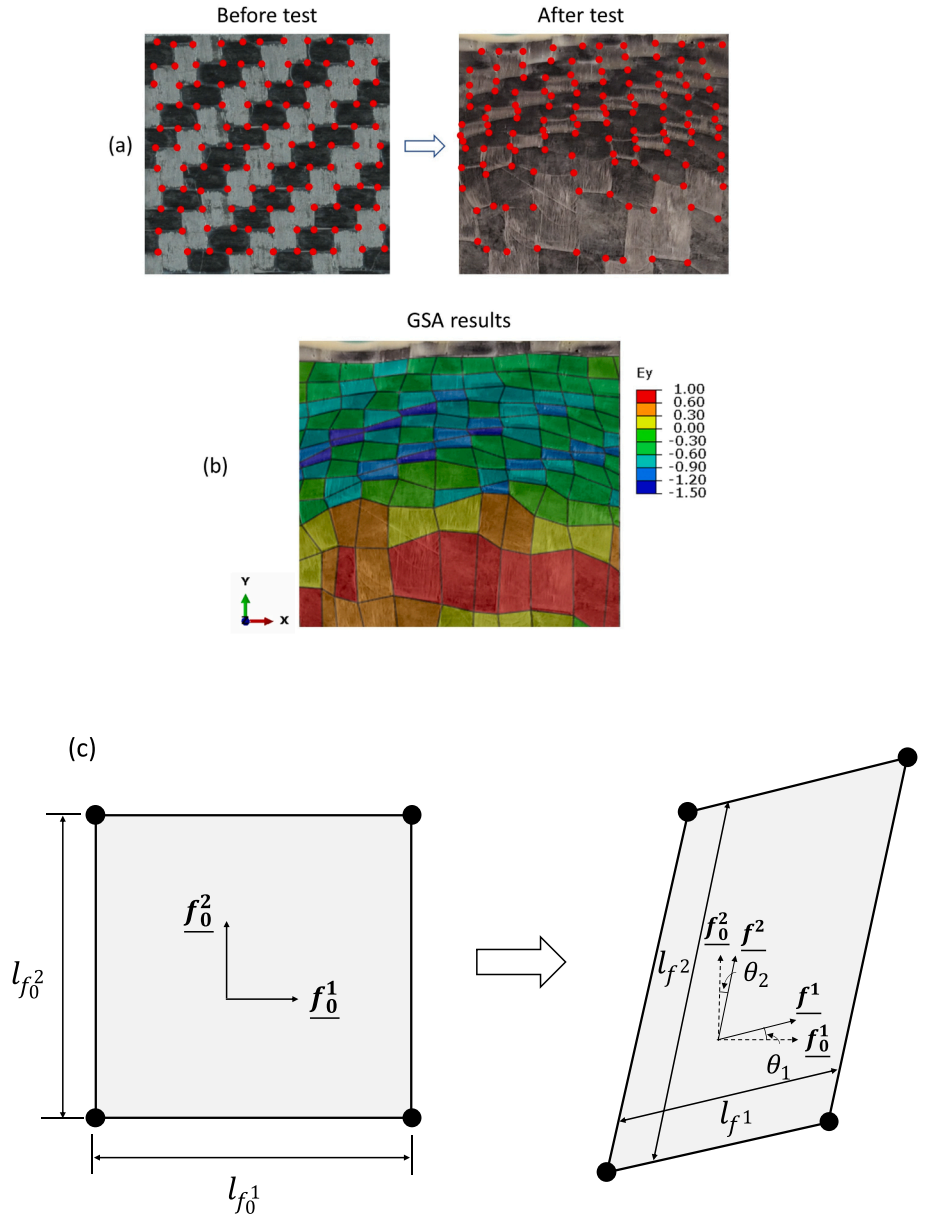

Fig. 15. (a) Example of nodes for GSA before and after the squeeze flow test; (b) in-plane strain results in second fibre direction (E_y) from GSA; (c) change of elemental dimensions and local fibre directions before and after the deformation.

is not in contact with the plate (not compacted) as demonstrated in Fig. 14. Therefore, higher flow resistance is caused by the prepreg in front of the flow front of the SMC as the SMC tends to sink into the prepreg, distorting the prepreg during flow. As a result, the pressure difference behind the flow front of the SMC (between -40 mm and -60 mm) towards the end of the test was much lower than that in the SMC-only test (Fig. 3 (b)) and the flow path of the SMC in the hybrid architecture test was more restricted compared to the SMC-only specimen.

A grid strain analysis (GSA) methodology was used to quantify the level of fibre tow distortion and deformation in the prepreg. Photographs of the prepreg-side of the specimen were taken before and after the test using an overhead camera mount. Corners and intersections of fibre tows in the photograph were picked as nodes of the grid and their coordinates were recorded and tracked (Fig. 15 (a) and (b)). It is worth noting that the local bending of fibre tows in the four-node grid element is not considered as the curvature observed from current experimental studies were negligible at this scale. The change in the angle between two fibre directions commonly called the shear angle is critical to the characterisation of deformations (i.e. the position and orientation of fibre tows) for woven fibrous materials. As shown in Fig. 15 (c), $\underline{f_0^1}$ and $\underline{f_0^2}$ are normalised local base vectors along initial first and second fibre directions, and $\underline{f^1}$ and $\underline{f^2}$ are normalised local base vectors along first and second fibre directions after the deformation. The in-plane shear angle γ of a deformed grid element can be calculated as [43]:

$$\gamma = \cos^{-1}\left(\frac{\underline{f_0^1} \bullet \underline{f_0^2}}{\|\underline{f_0^1}\| \bullet \|\underline{f_0^2}\|}\right) - \cos^{-1}\left(\frac{\underline{f^1} \bullet \underline{f^2}}{\|\underline{f^1}\| \bullet \|\underline{f^2}\|}\right) = \theta_1 + \theta_2 \tag{6}$$

The logarithmic strains E_x and E_y, representing the level of in-plane tow deformations in two fibre directions were calculated from the dimensions of the quadrilateral element regarding each fibre direction before ($l_{f_0^1}$ and $l_{f_0^2}$) and after the deformation (l_{f^1} and l_{f^2}) using nodal coordinates of the grid:

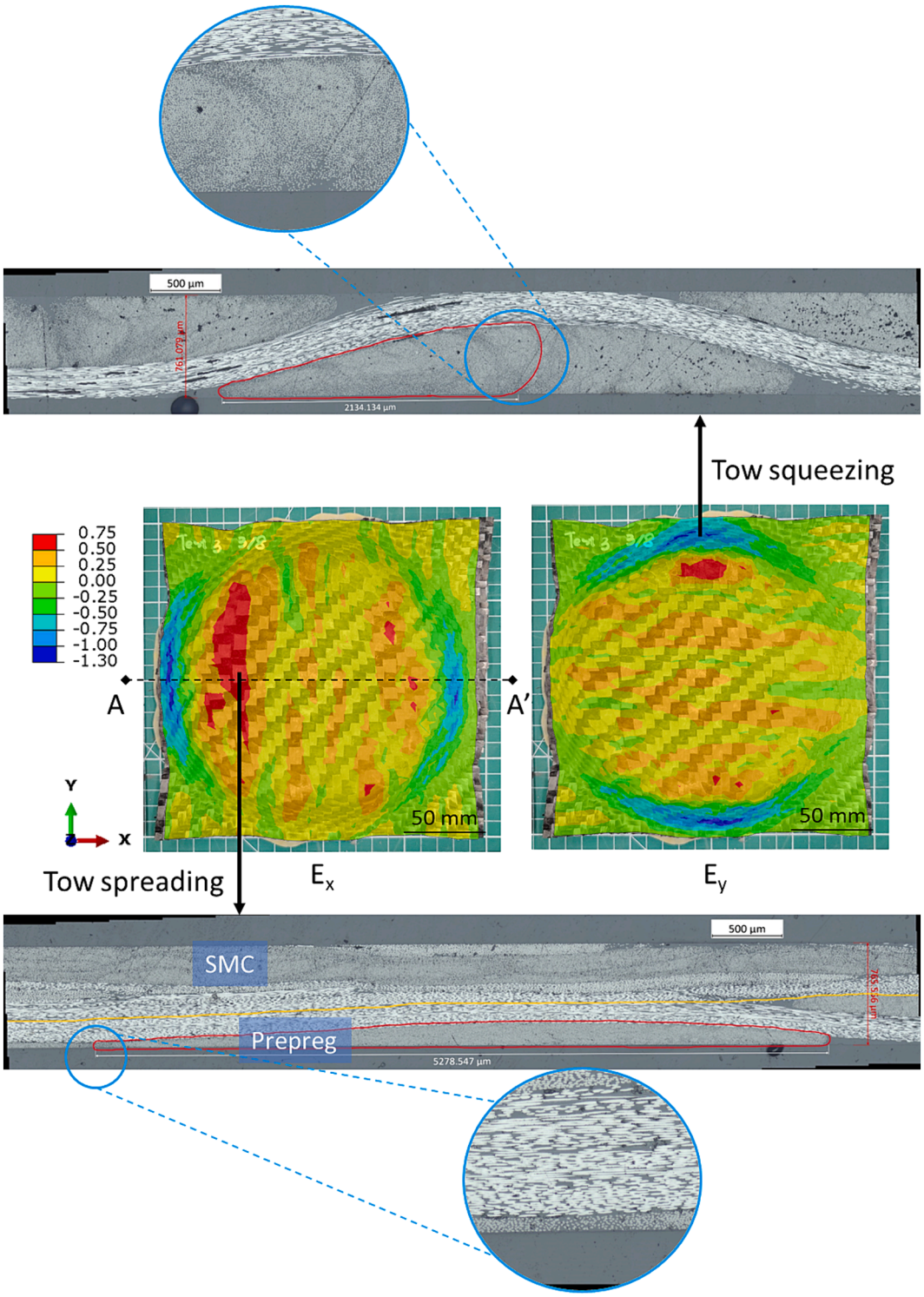

Fig. 16. In-plane strain in two fibre directions (E_x and E_y) for the woven prepreg in a hybrid architecture specimen. Micrographs of the cross-section highlight the regions with high strains. The boundaries of a fibre tow in the prepreg are highlighted in red. (For interpretation of the references to colour in this figure legend, the reader is referred to the web version of this article.)

$$E_x = \ln\left(l_{f^1}/l_{f_0^1}\right), E_y = \ln\left(l_{f^2}/l_{f_0^2}\right) \tag{7}$$

The simplified GSA approach adopted in this study eliminates the effects of rigid body motion by calculating strains from the elemental dimensions along the fibre directions. Colour contours in Fig. 16 are the in-plane strains of the woven prepreg in two fibre directions calculated using GSA. It can be seen that the highest level of tow deformations is concentrated in the region near the flow front of the SMC with tow spreading behind the flow front and tow compaction just ahead of the flow front. The micrographs in Fig. 16 show the cross-sections of the tow spreading and the tow compaction regions indicated in Fig. 12. The highlighted fibre tow behind the flow front of SMC increased more than 60 % in width from 3.5 mm to 5.3 mm while the fibre tows ahead of the flow front of SMC showed a 40 % decrease in width from 3.5 mm to 2.1

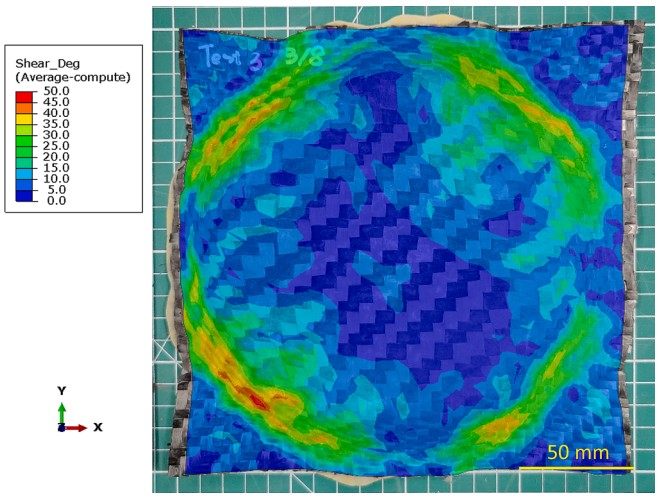

Fig. 17. Shear angle (degree) for the woven prepreg in a hybrid architecture specimen.

mm. In both cases, the boundaries of adjacent fibre tows can no longer be identified. In addition to tow compaction, high levels of in-plane shearing (>30°) in the prepreg can be observed in four corner areas just ahead of the SMC flow front as shown in Fig. 17, as a result of the radial flow of SMC (i.e. where both fibre directions were at a higher angle to the flow direction).

Three hybrid architecture specimens were tested under different maximum compressive forces for investigating tow distortions and deformations in woven fabric-based prepregs during the hybrid architecture test. These specimens were cut along the centre line, indicated as AA' on the specimen strain map in Fig. 16. The profile of the boundary line between SMC and prepreg was extracted from the micrographs in Fig. 16 to calculate local thicknesses and subsequently through-thickness strains (E_z) in the prepreg. The through-thickness strains along the cutline AA' for hybrid specimens subjected to different maximum compressive forces are compared in Fig. 18 with the in-plane strains (E_x) derived from GSA analysis. The location of x = 0 mm is

Table 2
Number of fibre tows suffering high in-plane strains ($E_x > 0.2$) for hybrid architecture tests at different compressive forces (x < 0 mm and x > 0 mm indicate two ends of the specimen).

Maximum compressive force	x < 0 mm		Centre	x > 0 mm	
	Squeezed	Spread		Spread	Squeezed
62 kN	5	5		4	6
104 kN	7	3		5	6
190 kN	9	5		5	9

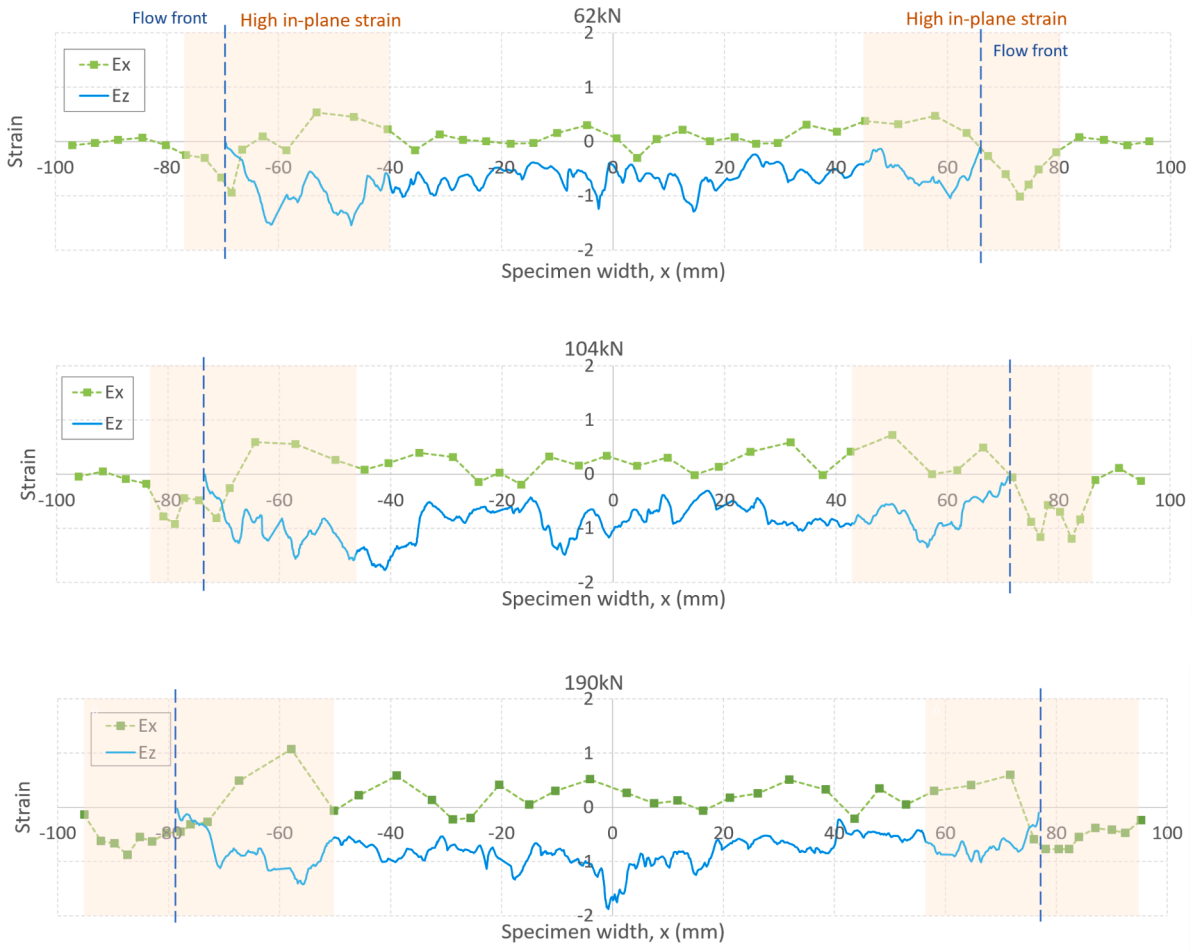

Fig. 18. In-plane strain (E_x) and through-thickness strain (E_z) along the cutline (AA') in Fig. 16 of three hybrid architecture specimens tested to 62 kN, 104 kN and 190 kN compressive forces (shaded areas represent regions with high in-plane strains and blue vertical dash line indicates the edge of SMC material). (For interpretation of the references to colour in this figure legend, the reader is referred to the web version of this article.)

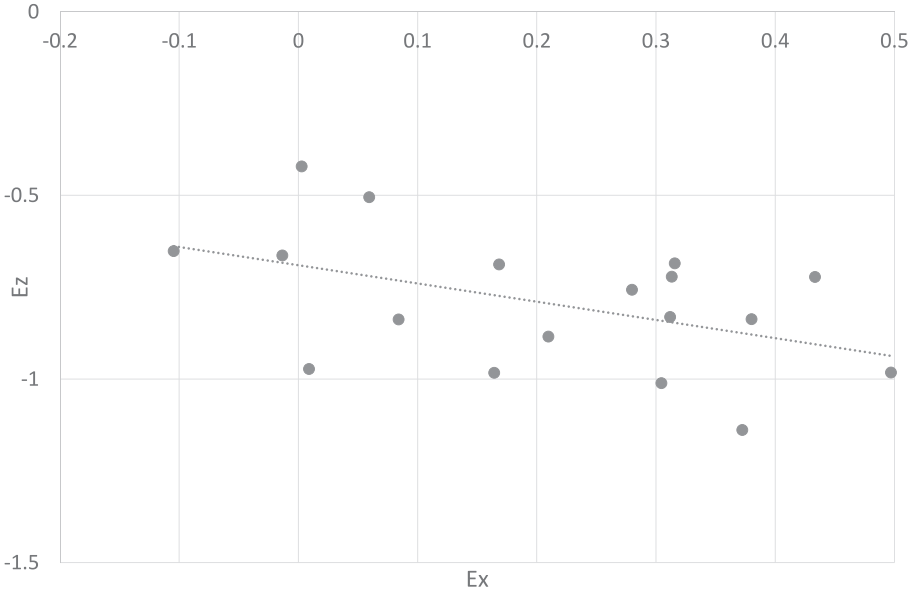

Fig. 19. Correlation between fibre tow in-plane strain (E_x) and through-thickness strain (E_z).

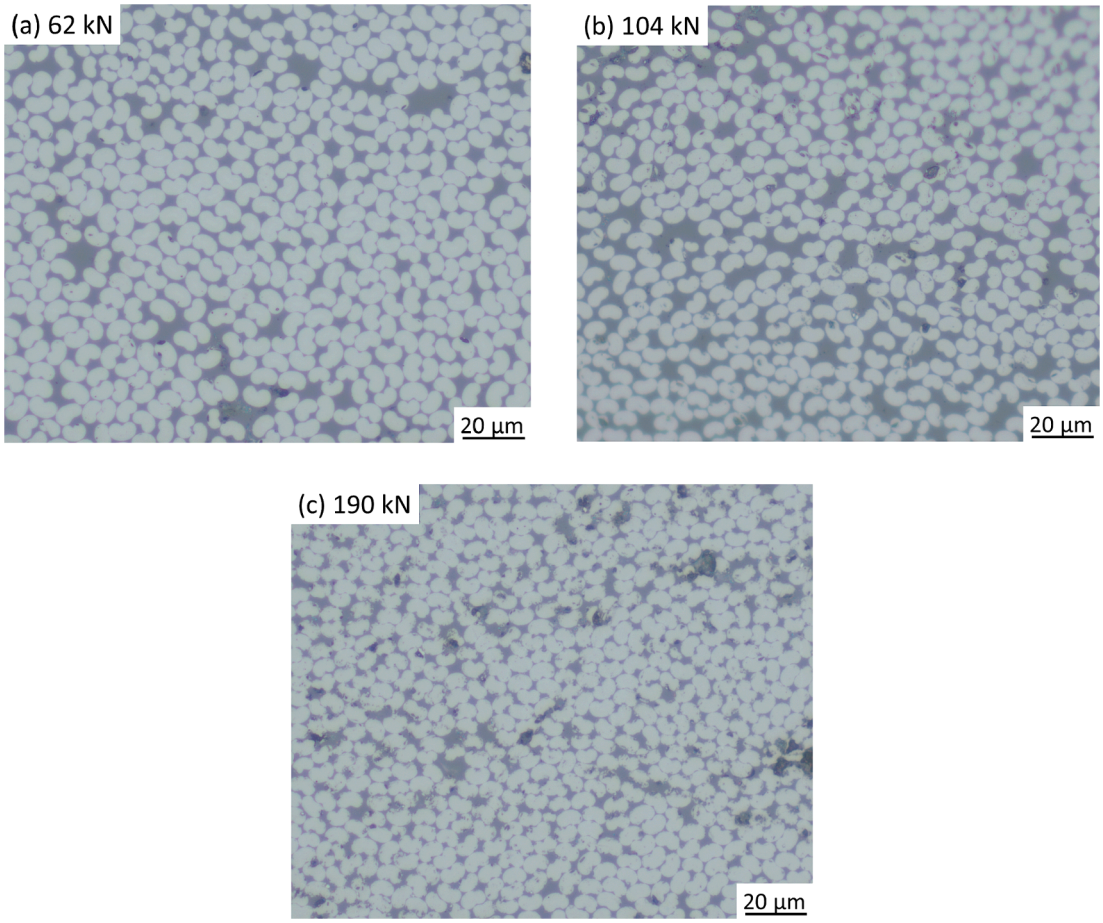

Fig. 20. High magnification micrographs of the cross-section of prepreg fibre tows at different levels of compressive forces in the hybrid architecture test.

located at the centre of the specimen. As indicated by the negative E_x, tow compaction in the prepreg material mainly took place ahead of the SMC flow front, whereas tow spreading was mainly observed (positive E_x) in the area directly underneath the SMC. The highest level of tow spreading (highest E_x) occurred just behind the SMC flow front. The level of tow spreading increases slightly from nearly zero E_x at 62 kN to 0.5 at 190 kN because of SMC flow as a result of increasing compressive force. Table 2 summarises the number of fibre tows experiencing high levels of compaction or spreading ($|E_x| > 0.2$) near the SMC flow front for specimens subjected to different maximum compressive forces. The

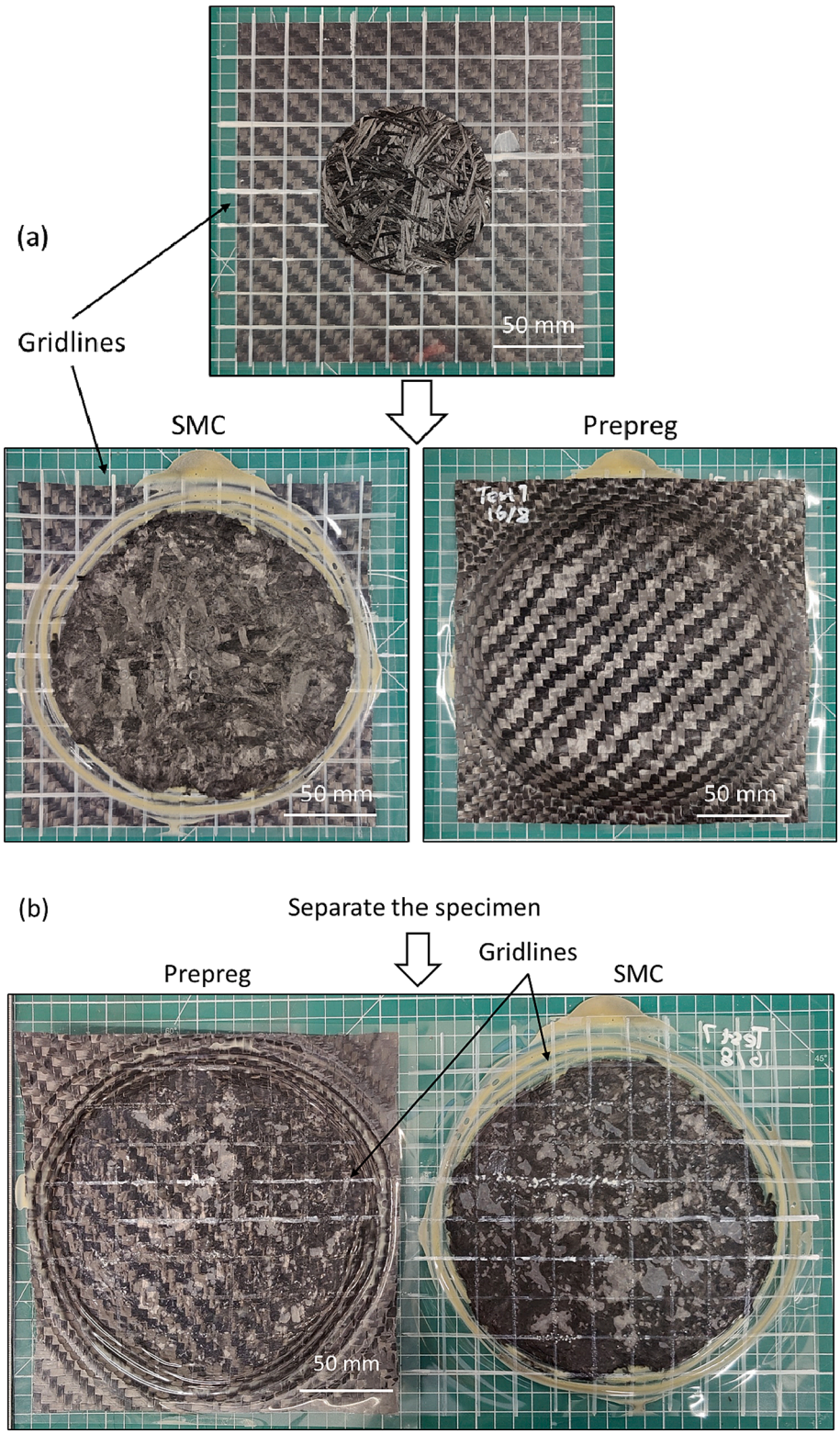

Fig. 21. (a) Hybrid-architecture specimen (configuration 3) with cellulose acetate films inserted to separate the prepreg and SMC and (b) the interface between the two materials.

number of highly deformed fibre tows increased with compressive force, indicating the expansion of the ring-shaped high-strain zone during the test.

Both E_x and E_z results presented in Fig. 18 were selected at an interval of 20 mm along the cutline and plotted in Fig. 19. Overall, E_x and E_z for the prepreg at three different force levels range from −0.1 to 0.5 and −0.3 to −1.8 across the area directly underneath the SMC. The scatter in this correlation may be attributed to the fact that E_x and E_z were measured at different resolutions due to different measuring techniques and points plotted here are average results over a distance. Additionally, the surface topology of the woven prepreg at the interface can still play a significant role in the level of through-thickness strain of

the prepreg (i.e. gaps and voids between fibre tows can always be subjected to higher compressive strains than those regions where tows cross over). Tests of hybrid architecture specimens containing multiple layers of woven prepreg may be able to reduce these effects and will be carried out shortly.

For each of these specimens, high magnification micrographs similar to those for prepreg-only specimens were taken for three fibre tows in the centre (within -20 mm $< x <$ 20 mm) in order to determine the average fibre volume fraction within the tows (Fig. 20). The fibre volume fraction results were plotted in Fig. 11 along with the tow width. The fibre volume fraction within a tow for hybrid architecture specimens remained at around 69 % to 72 % for three different levels of compaction pressures, which is slightly higher than those observed in the second stage of the prepreg-only tests (61 % to 63 %). This can be attributed to the further compaction of individual fibres and fibre tows, as observed from the reduced gaps between fibres and fibre tows in the micrographs. This also resulted in a slightly greater tow width in the hybrid architecture test (4.5 mm to 5.2 mm), compared to that observed in prepreg-only tests (4.2 mm). Results for the specimen at 11.4 MPa pressure did not follow a similar trend to the fibre volume fraction. This may be caused by the variability in specimens and tests.

Existing studies have claimed that in a hybrid moulding process, the deformation of fibre tows in the prepreg is mainly caused by the friction induced by the SMC flow [5,7]. A specifically designed experiment was performed in this paper to disprove this claim, where a hybrid architecture specimen test was performed with two layers of biaxially oriented cellulose acetate films inserted between the SMC and the prepreg. The thickness of one layer of film is 100 μm. Acetate films have a relatively high in-plane modulus (3 - 4 GPa), therefore the flow of the SMC will cause negligible in-plane deformation in the acetate film. This eliminates any frictional forces that can potentially drive the distortion of the prepreg, but only allows for the transfer of normal stresses through out-of-plane deformations in the acetate films. The reason that two layers of acetate films were used was to prove that there was negligible in-plane deformation in the films using a grid drawn onto each film prior to the test (Fig. 21 (a)), so that any in-plane deformation in the acetate films could be observed from the deformation of this grid. It is worth noting that theoretically only one film is required to achieve enough rigidity at the interface, however, two films were used in order to easily separate the two materials after the test. As shown in Fig. 21 (b), although there is wrinkling observed of the films ahead of the SMC flow front, the pre-drawn gridlines in the area directly under the SMC remained straight after the test, confirming that there was negligible in-plane deformation in the films. Meanwhile, the SMC and the prepreg experienced similar levels of deformations compared to the hybrid architecture specimen without the acetate films. This corroborates that the critical interaction mechanism between the two materials is the transfer of normal stresses, rather than friction.

4. Conclusions

A comprehensive characterisation of the deformation mechanisms for a fast-cure carbon fibre SMC and woven fabric-based prepreg in a hybrid moulding process was performed through squeeze flow tests. SMC and prepreg were tested individually as well as in a hybrid architecture under industry-relevant process conditions. The SMC showed a highly rate-dependent stress–strain response with similar squeeze flow behaviour under hybrid moulding conditions. The woven prepreg exhibited a bi-linear compressive stress–strain response with a 'hardening' type of transition at 2 MPa nominal pressure. In the high-pressure test, the fibre architecture showed a two-stage compaction response: First, tow spreading and a change in tow packing, leading to an increase in local fibre volume fraction, followed by a change in fibre tows' profile in the second stage along with squeeze flow effects near the edges of the specimen with fibre volume fraction remaining the same. When tested in hybrid architectures, additional deformation modes for woven fabric-based prepreg are fibre tow compaction ahead of the SMC flow front and extreme levels of tow spreading just after the SMC flow front which was not observed in the prepreg-only test. The test with two acetate films interleaved between the two composite materials confirmed that these extreme tow deformations are caused by the large normal stresses at the interface, while tangential stresses at the interface had negligible effect.

Further work will include further partial closure tests for all three specimen configurations at different force levels to examine the hypothesis of material compressibility at this stage. Pressure data from these tests will also be further analysed to help determine the contact area change and flow pattern. The stress–strain data acquired in this study will be used for the development or improvement of a suitable simulation models for compression moulding of the individual materials as well as hybrid architectures.

CRediT authorship contribution statement

Hao Yuan: Writing – original draft, Visualization, Validation, Methodology, Investigation, Formal analysis, Data curation, Conceptualization. **Muhammad Khan:** Validation, Writing – review & editing, Supervision, Resources. **Ton Peijs:** Writing – review & editing, Validation, Resources. **Connie Qian:** Writing – review & editing, Validation, Supervision, Resources, Project administration, Methodology, Investigation, Funding acquisition, Conceptualization.

Declaration of competing interest

The authors declare that they have no known competing financial interests or personal relationships that could have appeared to influence the work reported in this paper.

Data availability

Data will be made available on request.

Acknowledgements

The authors would like to express appreciation for the support of the EPSRC Future Composites Manufacturing Hub [EP/P006701/1] and the China Scholarship Council (CSC). The authors would also like to thank DowAksa for donating the materials used in this study, and for Jason Clarke, Paul Hadlum, Max Raybone and Neil Reynolds at WMG for their support in design and manufacture of the testing rig.

References

[1] Wulfsberg J, Herrmann A, Ziegmann G, Lonsdorfer G, Stöß N, Fette M. Combination of carbon fibre sheet moulding compound and prepreg compression moulding in aerospace industry. Procedia Eng 2014;81:1601–7. https://doi.org/10.1016/j.proeng.2014.10.197.

[2] Fette M, Hentschel M, Köhler F, Wulfsberg J, Herrmann A. Automated and cost-efficient production of hybrid sheet moulding compound aircraft components. Procedia Manuf 2016;6:132–9. https://doi.org/10.1016/j.promfg.2016.11.017.

[3] Visweswaraiah SB, Selezneva M, Lessard L, Hubert P. Mechanical characterisation and modelling of randomly oriented strand architecture and their hybrids - a general review. J Reinf Plast Compos 2018;37:548–80. https://doi.org/10.1177/0731684418754360.

[4] Gortner F, Medina L, Mitschang P. Influence of textile reinforcement on bending properties and impact strength of SMC-components. KMUTNB International Journal of Applied Science and Technology 2015;8:1–11. https://doi.org/10.14416/j.ijast.2015.07.005.

[5] Corbridge DM, Harper LT, De Focatiis DSA, Warrior NA. Compression moulding of composites with hybrid fibre architectures. Compos Part A Appl Sci Manuf 2017;95:87–99. https://doi.org/10.1016/j.compositesa.2016.12.018.

[6] Mallick PK. Effect of fiber misorientation on the tensile strength of compression molded continuous fiber composites. Polym Compos 1986;7:14–8. https://doi.org/10.1002/pc.750070104.

[7] Bücheler D. Locally Continuous-fiber Reinforced Sheet Molding Compound. Doctoral Thesis. Karlsruher Institut für Technologie (KIT), 2018. https://doi.org/10.5445/IR/1000079163.

[8] Zulueta K, Stelzer P, Rienesl K, Major Z, Vilas JL, Arrillaga A. Advancing on viscosity characterization and modeling of SMC for compression molding simulation. Polym Compos 2023:5567–78. https://doi.org/10.1002/pc.27510.
[9] Doppelbauer LK, Rienesl K, Stelzer PS, Zulueta K, Chang LY, Major Z. A macroscopic model of the compaction process during compression molding of carbon fiber sheet molding compounds. Compos Part A Appl Sci Manuf 2023;169:107535. https://doi.org/10.1016/j.compositesa.2023.107535.
[10] Kardos M, Körner E, Penumadu D, Modler N. The influence of fiber volume fraction and fiber length on the evolution of pore content and the paintability of sheet molding compounds. Compos B Eng 2020;185. https://doi.org/10.1016/j.compositesb.2020.107760.
[11] Zulueta K, Arriaga A, Martinez I. Novel coupon geometry for tensile property determination of sheet molding compounds. Mater Lett 2021;285. https://doi.org/10.1016/j.matlet.2020.129087.
[12] Silva-Nieto RJ, Fisher BC, Birley AW. Rheological characterization of unsaturated polyester resin sheet molding compound. Polym Eng Sci 1981;21:499–506. https://doi.org/10.1002/pen.760210810.
[13] Lee LJ, Marker LF, Griffith RM. The rheology and mold flow of polyester sheet molding compound. Polym Compos 1981;2:209–18. https://doi.org/10.1002/pc.750020412.
[14] Böhlke T, Henning F, Hrymak A, Kärger L, Weidenmann KA, Wood JT. Continuous discontinuous fiber reinforced polymers an integrated engineering approach. Munich: Hanser Publishers; 2019.
[15] Kotsikos G, Gibson AG. Investigation of the squeeze flow behaviour of sheet moulding compounds (SMC). Compos Part A Appl Sci Manuf 1998;29:1569–77. https://doi.org/10.1016/S1359-835X(98)00094-3.
[16] Comte E, Merhi D, Michaud V, Månson JAE. Void formation and transport during SMC manufacturing: effect of the glass fiber sizing. Polym Compos 2006;27:289–98. https://doi.org/10.1002/pc.20193.
[17] Guiraud O, Dumont PJJ, Orgéas L, Favier D. Rheometry of compression moulded fibre-reinforced polymer composites: rheology, compressibility, and friction forces with mould surfaces. Compos Part A Appl Sci Manuf 2012;43:2107–19. https://doi.org/10.1016/j.compositesa.2012.06.006.
[18] Lin CM, Weng CI, Ter HC. Anisotropy in sheet molding compounds during compression molding. Polym Compos 1997;18:613–22. https://doi.org/10.1002/pc.10312.
[19] Castro JM, Tomlinson G. Predicting molding forces in SMC compression molding. Polym Eng Sci 1990;30:1568–73. https://doi.org/10.1002/pen.760302403.
[20] Dumont P, Orgéas L, Le Corre S, Favier D. Anisotropic viscous behavior of sheet molding compounds (SMC) during compression molding. Int J Plast 2003;19:625–46. https://doi.org/10.1016/S0749-6419(01)00077-8.
[21] Toll S. Packing mechanics of fiber reinforcements. Polym Eng Sci 1998;38:1337–50. https://doi.org/10.1002/pen.10304.
[22] Morris JF. Shear thickening of concentrated suspensions: recent developments and relation to other phenomena. Annu Rev Fluid Mech 2020;52:121–44. https://doi.org/10.1146/annurev-fluid-010816-060128.
[23] Hubert P, Poursartip A. A review of flow and compaction modelling relevant to thermoset matrix laminate processing. J Reinf Plast Compos 1998;17:286–318. https://doi.org/10.1177/073168449801700402.
[24] Chen B, Chou TW. Compaction of woven-fabric preforms in liquid composite molding processes: single-layer deformation. Compos Sci Technol 1999;59:1519–26. https://doi.org/10.1016/S0266-3538(99)00002-0.
[25] Chen B, Chou TW. Compaction of woven-fabric preforms: nesting and multi-layer deformation. Compos Sci Technol 2000;60:2223–31. https://doi.org/10.1016/S0266-3538(00)00017-8.
[26] Comas-Cardona S, Le Grognec P, Binetruy C, Krawczak P. Unidirectional compression of fibre reinforcements. Part 1: a non-linear elastic-plastic behaviour. Compos Sci Technol 2007;67:507–14. https://doi.org/10.1016/j.compscitech.2006.08.017.
[27] Nixon-Pearson OJ, Belnoue JPH, Ivanov DS, Potter KD, Hallett SR. An experimental investigation of the consolidation behaviour of uncured prepregs under processing conditions. J Compos Mater 2017;51:1911–24. https://doi.org/10.1177/0021998316665681.
[28] Belnoue JPH, Nixon-Pearson OJ, Ivanov D, Hallett SR. A novel hyper-viscoelastic model for consolidation of toughened prepregs under processing conditions. Mech Mater 2016;97:118–34. https://doi.org/10.1016/j.mechmat.2016.02.019.
[29] Rashidi A, Belnoue J-P-H, Thompson AJ, Hallett SR, Milani AS. Consolidation-driven wrinkling in carbon/epoxy woven fabric prepregs: an experimental and numerical study. Compos Part A Appl Sci Manuf 2021;143:106298. https://doi.org/10.1016/j.compositesa.2021.106298.
[30] Sorba G, Binetruy C, Leygue A, Comas-Cardona S. Squeeze flow in heterogeneous unidirectional discontinuous viscous prepreg laminates: Experimental measurement and 3D modeling. Compos Part A Appl Sci Manuf 2017;103:196–207. https://doi.org/10.1016/j.compositesa.2017.10.007.
[31] Hautefeuille A, Comas-Cardona S, Binetruy C. Mechanical signature and full-field measurement of flow-induced large in-plane deformation of fibrous reinforcements in composite processing. Compos Part A Appl Sci Manuf 2019;118:213–22. https://doi.org/10.1016/j.compositesa.2018.12.030.
[32] Hautefeuille A, Comas-Cardona S, Binetruy C. Consolidation and compression of deformable impregnated fibrous reinforcements: Experimental study and modeling of flow-induced deformations. Compos Part A Appl Sci Manuf 2020;131:105768. https://doi.org/10.1016/j.compositesa.2020.105768.
[33] Yong AXH, Aktas A, May D, Endruweit A, Lomov SV, Advani S, et al. Experimental characterisation of textile compaction response: a benchmark exercise. Compos Part A Appl Sci Manuf 2021;142. https://doi.org/10.1016/j.compositesa.2020.106243.
[34] Romanenko V, Duhovic M, Schommer D, Hausmann J, Eschl J. Advanced process simulation of compression molded carbon fiber sheet molding compound (C-SMC) parts in automotive series applications. Compos Part A Appl Sci Manuf 2022;157:106924. https://doi.org/10.1016/j.compositesa.2022.106924.
[35] Orgéas L, Dumont PJJ. Sheet molding compounds. Wiley encyclopedia of composites. Wiley 2012:1–36. https://doi.org/10.1002/9781118097298.weoc222.
[36] Reichanadter A, Dustin JS, Balijepalli B, Mansson JA. Process modeling and flexible manufacturing of multi-phase resin based thermoset and thermoplastic prepreg. In: Automotive composites conference & exhibition, Novi, MI: SPE automotive and composites divisions; 2018. p. 1–11.
[37] Barone MR, Caulk DA. A model for the flow of a chopped fiber reinforced polymer compound in compression molding. J Appl Mech 1986;53:361–71. https://doi.org/10.1115/1.3171765.
[38] Odenberger PT, Andersson HM, Lundström TS. Experimental flow-front visualisation in compression moulding of SMC. Compos Part A Appl Sci Manuf 2004;35:1125–34. https://doi.org/10.1016/j.compositesa.2004.03.019.
[39] Hohberg M, Kärger L, Henning F, Hrymak A. Rheological measurements and rheological shell model considering the compressible behavior of long fiber reinforced sheet molding compound (SMC). Compos Part A Appl Sci Manuf 2017;95:110–7. https://doi.org/10.1016/j.compositesa.2017.01.006.
[40] Görthofer J, Meyer N, Pallicity TD, Schöttl L, Trauth A, Schemmann M, et al. Virtual process chain of sheet molding compound: development, validation and perspectives. Compos B Eng 2019;169:133–47. https://doi.org/10.1016/j.compositesb.2019.04.001.
[41] Waterbury MC, Drzal LT. Determination of fiber volume fractions by optical numeric volume fraction analysis. J Reinf Plast Compos 1989;8:627–36. https://doi.org/10.1177/073168448900800605.
[42] Hubert P, Poursartip A. A method for the direct measurement of the fibre bed compaction curve of composite prepregs. Compos Part A Appl Sci Manuf 2001;32:179–87. https://doi.org/10.1016/S1359-835X(00)00143-3.
[43] Khan MA, Mabrouki T, Vidal-Sallé E, Boisse P. Numerical and experimental analyses of woven composite reinforcement forming using a hypoelastic behaviour. application to the double dome benchmark. J Mater Process Technol 2010;210:378–88. https://doi.org/10.1016/j.jmatprotec.2009.09.027.